ADVANCES IN ATMOSPHERIC SCIENCES, VOL. 41, JANUARY 2024, 73–83

• **Original Paper** •

Diagnosis of the Kinetic Energy of the "21·7" Extreme Torrential Rainfall Event in Henan Province, China

Xiuping YAO*[1,2], Ruoying LI[2,1], Xiaohong BAO[3,2,1], and Qiaohua LIU[3,2,1]

[1]*China Meteorological Administration Training Centre*, *Beijing* 100081, *China*

[2]*State Key Laboratory of Severe Weather*, *Chinese Academy of Meteorological Sciences*, *Beijing* 100081, *China*

[3]*College of Atmospheric Sciences*, *Nanjing University of Information Science and Technology*, *Nanjing* 210044, *China*

(Received 8 February 2023; revised 7 May 2023; accepted 9 May 2023)

ABSTRACT

An extreme torrential rain (ETR) event occurred in Henan Province, China, during 18-21 July 2021. Based on hourly rain-gauge observations and ERA5 reanalysis data, the ETR was studied from the perspective of kinetic energy (K), which can be divided into rotational wind ($\mathbf{V}_R$) kinetic energy (K_R), divergent wind kinetic energy (K_D), and the kinetic energy of the interaction between the divergent and rotational winds (K_{RD}). According to the hourly precipitation intensity variability, the ETR process was divided into an initial stage, a rapid increase stage, and maintenance stage. Results showed that the intensification and maintenance of ETR were closely related to the upper-level K, and most closely related to the upper-level K_R, with a correlation coefficient of up to 0.9. In particular, the peak value of hourly rainfall intensity lagged behind the K_R by 8 h. Furthermore, diagnosis showed that K transformation from unresolvable to resolvable scales made the ETR increase slowly. The meridional rotational wind (u_R) and meridional gradient of the geopotential (φ) jointly determined the conversion of available potential energy (APE) to K_R through the barotropic process, which dominated the rapid enhancement of K_R and then caused the rapid increase in ETR. The transportation of K by rotational wind consumed K_R, and basically offset the K_R produced by the barotropic process, which basically kept K_R stable at a high value, thus maintaining the ETR.

Key words: extreme torrential rain, rotational kinetic energy, kinetic energy generation and transport, barotropic process

Citation: Yao, X. P., R. Y. Li, X. H. Bao, and Q. H. Liu, 2024: Diagnosis of the kinetic energy of the "21·7" extreme torrential rainfall event in Henan Province, China. *Adv. Atmos. Sci.*, **41**(1), 73−83, https://doi.org/10.1007/s00376-023-3025-6.

Article Highlights:

- The intensification and maintenance of ETR were closely related to the upper-level K and most closely related to the upper-level K_R.
- The u_R and meridional gradient of φ jointly determined the conversion of APE to K_R, which dominated the rapid enhancement of K_R and ETR.
- Transportation of K by $\mathbf{V}_R$ consumed K_R and cancelled the K_R produced by the barotropic process, which maintained both the K_R and ETR.

1. Introduction

During 18–22 July 2021, a rarely seen extreme torrential rainfall (ETR) event occurred in Henan Province, China, where the human population density and levels of agricultural activity are high (hereafter referred to as the "21·7" ETR), the maximum hourly precipitation of which set a new record for the Chinese mainland, reaching 201.9 mm (Su et al., 2021; Zhang et al., 2021; Chyi et al., 2022). The 21·7 ETR caused heavy human casualties and losses of property, resulting in 398 deaths or missing persons and a direct economic loss in Henan Province exceeding RMB 120 billion (Disaster Investigation Group of the State Council, 2022). Therefore, the causes of the 21·7 ETR have become a key focus of meteorologists.

Previous studies have indicated that the 21·7 ETR was generated by the combined action of multiscale weather systems at different heights of the troposphere superimposed with topographic effects (Ran et al., 2021; Zhang et al., 2021; Cai et al., 2022; Chyi et al., 2022; Deng et al., 2022; Duan et al., 2022; Fu et al., 2022; Liang et al., 2022; Xu

* Corresponding author: Xiuping YAO
Email: yaoxp@cma.gov.cn

et al., 2022a; Zhu et al., 2022) in the context of extreme daily circulation (Xu et al., 2022b; Zhang et al., 2022), while the south–north shifting of the rainfall was related to the varying direction of low-level jets in the boundary layer (Luo and Du, 2023). Warming may lead to significant intensification of both regional-scale and station-scale precipitation extremes, and squall-line convection results in much higher precipitation extremes at both regional and station scales than unorganized convection (Qin et al., 2022). The abnormal northward shift of the western Pacific subtropical high along with the binary typhoon system of Typhoon In-Fa (2021) and Typhoon Cempaka (2021) jointly drove water vapor transportation and convergence in Henan (Sun et al., 2021; Bueh et al., 2022; Wang et al., 2022), where water vapor mainly originates from southern China and the western North Pacific (Nie and Sun, 2022), with the contribution of the former (52.51%) double that of the latter (25.51%) (Cui and Yang, 2022). At the same time, there were also large quantities of hydrometeors transported to the updraft area, which may have greatly accelerated the microphysical process of water vapor transformation into cloud water droplets and, ultimately, precipitation (Chen et al., 2022). Furthermore, the updrafts of the arc-shaped convergence zone may also have attracted all associated precipitation that was overlaid and concentrated into the same trailing region of the convective system to generate the extreme hourly rainfall over Zhengzhou (Yin et al., 2022). The abnormally strong vertical motion (Zhang et al., 2021, 2023) was caused by dynamic forcing, diabatic forcing, and topographic forcing, of which diabatic forcing contributed the most, while topographic forcing contributed to the vertical motion of the lower layer (Zhao et al., 2022).

The 21·7 ETR event was accompanied by drastic variations in the horizontal wind field (Zhang et al., 2022; Luo and Du, 2023), which can be decomposed into the divergent and rotational winds, thereby providing more information on the relationship between the structural changes in the horizontal wind fields and strengthening of the rainstorm (Deng et al., 2012). Diagnosing the kinetic energy budget is an effective way to analyze the sources and sinks of horizontal wind variations. Correspondingly, the kinetic energy can be decomposed into divergent and rotational kinetic energies and the kinetic energy of interaction between the divergent wind and the rotational wind (Fuelberg and Browning, 1983; Buechler and Fuelberg, 1986). Through this decomposition method, we can understand the role of each component of kinetic energy in the kinetic energy balance and the specific process of their respective generation, transport, and interconversion. In this way, we can obtain a deeper understanding of the kinetic energy of rainstorms.

Diagnosis of the divergent and rotational kinetic energies has been applied in the study of many systems related to heavy rainfall, such as tropical cyclones (Ding and Liu, 1985; Wang et al., 2016), extratropical cyclones (Pearce, 1974), the mei-yu system (Xie et al., 1980; Wang and Liu, 1994; Fu et al., 2016), upper- and lower-level jets (Zhong et al., 2021), and low vortexes (Sun et al., 1993; Fu et al., 2011), with many meaningful results having been obtained. Rotational kinetic energy is generally dominant in the formation and development stages of weather systems associated with precipitation (Duan et al., 1997; Zhong et al., 2021). There is a certain relationship between the horizontal flux divergence of rotational kinetic energy in the area of a typhoon and the enhancement of its heavy rainfall (Li and Shou, 1995). In addition, divergent kinetic energy acts as a catalyst in the conversion between available potential energy (APE) and rotational kinetic energy (Wang, 1993, Wang and Liu, 1994; Yu and Yao, 1999; Cheng et al., 2014). The conversion of divergent kinetic energy to rotational kinetic energy can contribute to an increase in rotational kinetic energy (Sha et al., 2018), which is conducive to the development of torrential rain (Jin et al., 2020; Bao and Yao, 2022).

However, the relationship between the divergent and rotational kinetic energies and the development and maintenance mechanism in the 21·7 ETR has not yet been studied. Accordingly, we studied the 21·7 ETR from the perspective of kinetic energy to explore the sources and sinks of the wind variations surrounding it, the aim being to improve our understanding of the development and maintenance mechanism of the 21·7 ETR.

The remainder of the paper is organized as follows. The data and methods employed in our study are introduced in section 2. Section 3 presents the relationship of the ETR event with the kinetic energies and the development and maintenance mechanism for this particular case. Finally, conclusions and some further discussion are provided in section 4.

2. Data and methods

2.1. *Data*

This study used hourly precipitation data from 0800 LST [Local Standard Time, which is eight hours ahead of coordinated universal time (UTC)] on 18 July to 0800 LST on 21 July 2021 provided by the National Meteorological Information Center of the China Meteorological Administration. In addition, the hourly horizontal wind, vertical velocity, and geopotential height during the same period were also used, which were derived from fifth major global reanalysis produced by ECMWF (ERA5). The hourly reanalysis dataset had a horizontal resolution of $0.25° \times 0.25°$ and 27 layers from 1000 hPa to 100 hPa in the vertical direction (Hersbach et al., 2020).

2.2. *Methods*

The horizontal wind ($\mathbf{V}$) was decomposed into the rotational wind ($\mathbf{V}_R$) and divergent wind ($\mathbf{V}_D$) by adopting the Endlich method, and the derivatives were calculated using centered finite differences (Endlich, 1967). The method works easily and has high precision, as it does not use the relationships between the stream function and vorticity function to solve Poisson equations and is independent of boundary conditions. The main idea of this method is to iteratively

adjust the rotational wind to make its horizontal divergence gradually tend towards zero, and its vertical component of the relative vorticity (ζ) should meet the requirements of the ζ of the original wind field, to successfully obtain the rotational wind, and then the rotational wind is subtracted from the original wind field to obtain the divergent wind. In this iterative process, the divergence error at each grid point is less than or equal to 1×10^{-8} s^{-1}; that is, less than or equal to 0.001% of the maximum divergence of the original horizontal wind field.

Kinetic energy per unit mass can be decomposed into

$$k = k_{\mathrm{R}} + k_{\mathrm{D}} + k_{\mathrm{RD}}\,, \tag{1}$$

where

$$\begin{cases} k = \dfrac{1}{2}\mathbf{V}\cdot\mathbf{V} \\ k_{\mathrm{R}} = \dfrac{1}{2}\mathbf{V_R}\cdot\mathbf{V_R} \\ k_{\mathrm{D}} = \dfrac{1}{2}\mathbf{V_D}\cdot\mathbf{V_D} \\ k_{\mathrm{RD}} = \mathbf{V_R}\cdot\mathbf{V_D} \end{cases}. \tag{2}$$

The kinetic energy of an atmospheric volume in isobaric coordinates (A being the horizontal limited computational area) is calculated as follows:

$$K = K_{\mathrm{D}} + K_{\mathrm{R}} + \iint \mathbf{V}_{\mathrm{R}}\cdot\mathbf{V}_{\mathrm{D}} = K_{\mathrm{D}} + K_{\mathrm{R}} + K_{\mathrm{RD}}\,, \tag{3}$$

where

$$\begin{cases} K = \iint k \\ K_{\mathrm{R}} = \iint k_{\mathrm{R}} \\ K_{\mathrm{D}} = \iint k_{\mathrm{D}} \\ K_{\mathrm{RD}} = \iint k_{\mathrm{RD}} \\ \iint = \dfrac{1}{gA}\iiint \mathrm{d}x\mathrm{d}y\mathrm{d}p \end{cases}. \tag{4}$$

Here, K is the kinetic energy of a limited region (hereinafter simply referred to as "kinetic energy"), K_{D} is the divergent kinetic energy, K_{R} is the rotational kinetic energy, and K_{RD} is the kinetic energy of the interaction between the divergent and rotational winds. K_{D}, K_{R}, and K_{RD} are all defined in a limited region.

The budget equation for K_{R} (Buechler and Fuelberg, 1986) is expressed as follows:

$$\underset{\mathrm{DK_R}}{\frac{\partial K_{\mathrm{R}}}{\partial t}} = \underset{\mathrm{I_R}}{\iint -\mathbf{V}_{\mathrm{R}}\cdot\frac{\partial \mathbf{V}_{\mathrm{D}}}{\partial t}} + \underset{\mathrm{Af}}{\iint -f(v_{\mathrm{R}}u_{\mathrm{D}} - u_{\mathrm{R}}v_{\mathrm{D}})} + \underset{\mathrm{Az}}{\iint -\zeta(v_{\mathrm{R}}u_{\mathrm{D}} - u_{\mathrm{R}}v_{\mathrm{D}})} + \underset{\mathrm{B}}{\iint -\omega\frac{\partial k_{\mathrm{R}}}{\partial p}} + \underset{\mathrm{C}}{\iint -\omega\mathbf{V}_{\mathrm{R}}\cdot\frac{\partial \mathbf{V}_{\mathrm{D}}}{\partial p}} + \underset{\mathrm{G_R}}{\iint -\mathbf{V}_{\mathrm{R}}\cdot\nabla\varphi} + \underset{\mathrm{HF_R}}{\iint -\nabla\cdot k\mathbf{V}_{\mathrm{R}}} + \underset{\mathrm{F_R}}{\iint -\mathbf{V}_{\mathrm{R}}\cdot\mathbf{F}}\,. \tag{5}$$

Here, u_{R} and v_{R} are the zonal and meridional components of the rotational wind, respectively. Similarly, u_{D} and v_{D} are the zonal and meridional components of the divergent wind, respectively. Further, ζ is the vertical component of the relative vorticity, ω is the vertical velocity (units: Pa s^{-1}), f is the Coriolis parameter, φ is the geopotential, and $\mathbf{F}$ is the frictional force.

The sum of terms Af, Az, B, and C is denoted as C(K_{D}, K_{R}). Therefore, Eq. (5) can be simplified as $\mathrm{DK_R} = \mathrm{I_R} + \mathrm{C}(K_{\mathrm{D}}, K_{\mathrm{R}}) + \mathrm{G_R} + \mathrm{HF_R} + \mathrm{F_R}$. The term on the left-hand side denotes the local change in K_{R}. The term $\mathrm{I_R}$ represents the change in K_{R} caused by the nonlinear interaction between the rotational and divergent winds. Term Af is to satisfy the conservation of angular momentum on the tangential motion and is called the geostrophic effect term. Term Az is to satisfy the conservation of angular momentum on the rotational motion. Both Af and Az are affected by the relative magnitudes and orientations of $\mathbf{V}_{\mathrm{R}}$ and $\mathbf{V}_{\mathrm{D}}$. Term B describes the vertical exchange of K_{R}, while term C is related to the configuration of $\mathbf{V}_{\mathrm{D}}$ with $\mathbf{V}_{\mathrm{R}}$ and the vertical distribution of $\mathbf{V}_{\mathrm{D}}$. The term C(K_{D}, K_{R}) denotes the conversion between K_{D} and K_{R}, where a positive value indicates a conversion from K_{D} to K_{R} and a negative value indicates the opposite. Term $\mathrm{G_R}$ is the generation term for K_{R}, indicating the conversion between the APE and K_{R} due to the cross-contour flow of $\mathbf{V}_{\mathrm{R}}$. Term $\mathrm{HF_R}$ is the transportation term for K_{R}, indicating the horizontal transportation of K by $\mathbf{V}_{\mathrm{R}}$. Term $\mathrm{F_R}$ is the friction term related to $\mathbf{V}_{\mathrm{R}}$, including frictional processes and the energy transfer between the sub-grid scale and the grid scale of motion. As $\mathrm{F_R}$ is calculated as the residual, it includes possible errors from other terms in Eq. (5). For analyzing the balance of the budget equation for K_{R}, we calculated the average ratio of the right-hand side terms (except term $\mathrm{F_R}$) to the left-hand side term $\mathrm{DK_R}$ as 3.46, which is reasonable compared with an earlier study using the same equation (Buechler and Fuelberg, 1986).

3. Results

3.1. *Stages of the ETR event*

During 18–21 July 2021, torrential rainfall occurred in most areas of Henan Province, with the accumulated precipitation exceeding 800 mm (3 d)$^{-1}$ (Fig. 1a). From the day-by-

day distribution of precipitation in Fig. 1, the rainstorm range was concentrated and relatively static, but the intensity was increasing. On 18 July, the heavy rainfall was mainly distributed in the northern part of Henan Province (Fig. 1b). On 19 July, the range of heavy rainfall expanded, with the maximum daily precipitation exceeding 400 mm d^{-1} (Fig. 1c); and on 20 July, the range of heavy rainfall continued to expand, with the range of daily precipitation exceeding 250 mm d^{-1}, reaching a maximum, and the maximum daily precipitation exceeding 600 mm d^{-1} (Fig. 1d). From Fig. 1, the precipitation during the ETR event was concentrated in the region of (32.5°–37°N, 111.5°–115.5°E). Therefore, this region was identified as the key region in this research, which we refer to as the torrential-rain area (red dashed frame in Fig. 1).

Figure 2 shows the temporal evolution of hourly precipitation (also called the hourly rain intensity) within the torrential-rain area during 18–21 July, from which we can see that the hourly precipitation in that period enhanced with time. On 18 July, the hourly average precipitation increased by 0.05 mm h^{-1} and the average hourly precipitation was 0.93 mm h^{-1}. On 19 July, the hourly average precipitation increased by 0.09 mm h^{-1} and the average hourly precipitation was 2.02 mm h^{-1}. On 20 July, the hourly average precipitation increased by 0.01 mm h^{-1} and the average hourly precipitation was 3.43 mm h^{-1}. The average hourly precipitation was largest on 20 July, second largest on 19 July, and smallest on 18 July. Also, the hourly average precipitation increased the most on 19 July, second most on 18 July, and least on 20 July.

To comprehensively assess the average hourly precipitation and hourly rainfall intensity variability, the ETR event was divided into three stages: the initial stage, from 0800 LST 18 to 0800 LST 19 July 2021; the rapid increase stage, from 0800 LST 19 to 0800 LST 20 July 2021; and the maintenance stage, from 0800 LST 20 to 0800 LST 21 July 2021.

3.2. *Spatial and temporal distribution of kinetic energy*

Figure 3 shows the vertical profile of the regional average K, K_R, K_D, and K_{RD} in the torrential-rain area. In the torrential-rain area, the vertical totals of K were closely related to the hourly precipitation, with their correlation coefficients being greater than 0.6 (figure omitted). The vertical distributions of K, K_R, K_D, and K_{RD} show a bimodal pattern in the initial, rapid increase, and maintenance stages of the ETR event, with the main peak and secondary peak at around 200 hPa and 800 hPa, respectively (Fig. 3). Also, as the main and secondary peak values increase, the ETR strengthens accordingly (Fig. 3). In Fig. 3, K and K_R are basically the same, and the values of K_D and K_{RD} are small and mostly around zero. The peaks of K and K_R at 200 hPa are 43 J m^{-2} and 36 J m^{-2}, respectively, during the initial stage (Fig. 3a), increasing to 96 J m^{-2} and 88 J m^{-2} during the rapid increase stage (Fig. 3b), and both exceeding 100 J m^{-2} during the maintenance stage (Fig. 3c), with K_R increasing to

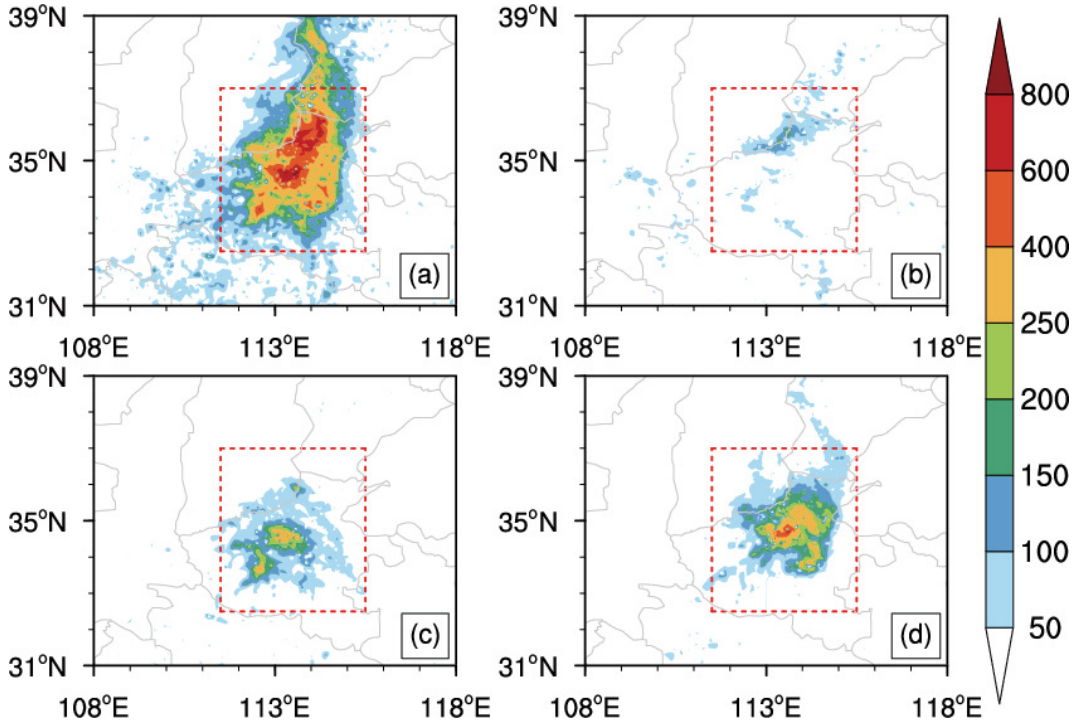

Fig. 1. Distribution of accumulated precipitation during (a) 0800 LST 18 July to 0800 LST 21 July 2021 [shaded; units: mm $(3\ d)^{-1}$], (b) 0800 LST 18 July to 0800 LST 19 July 2021 (shaded; units: mm d^{-1}), (c) 0800 LST 19 July to 0800 LST 20 July 2021 (shaded; units: mm d^{-1}), and (d) 0800 LST 20 July to 0800 LST 21 July 2021 (shaded; units: mm d^{-1}). The red dashed frame represents the torrential-rain area (32.5°–37°N, 111.5°–115.5°E; the same in subsequent figures).

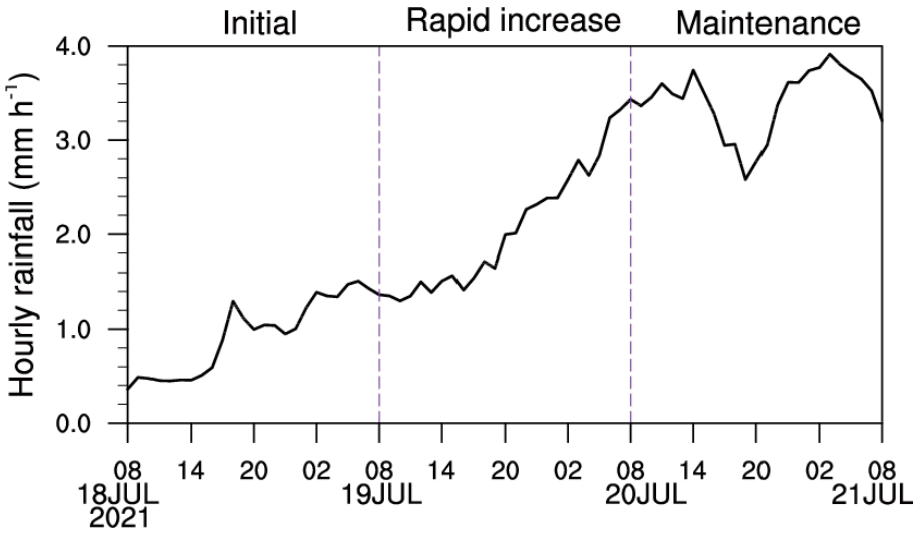

Fig. 2. Temporal evolution of the regional-mean hourly precipitation within the torrential-rain area from 0800 LST 18 July to 0800 LST 21 July 2021 (units: mm h^{-1}).

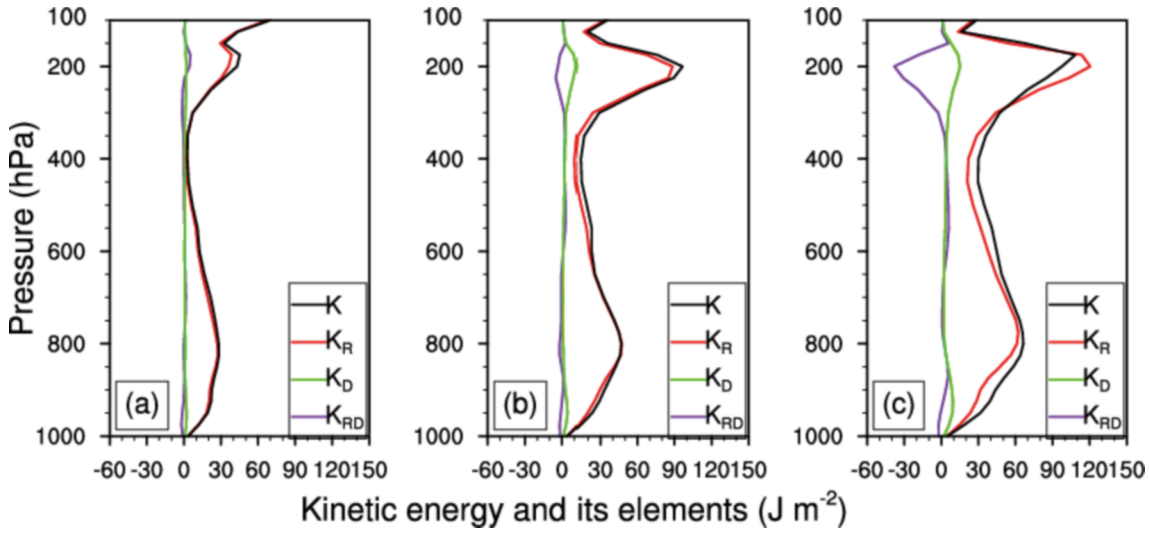

Fig. 3. Vertical profiles of area-averaged K, K_R, K_D, and K_{RD} (units: J m^{-2}) in the (a) initial stage, (b) rapid increase stage, and (c) maintenance stage.

120 J m^{-2}. The reason why K_R is greater than K during the maintenance stage is that K_{RD} decreases to −30 J m^{-2} and thus K is weakened. During the ETR process, although the K and K_R values at 800 hPa also increase, their changes are less than half of those at 200 hPa.

It can be seen that K is enhanced during the ETR, and the ETR thus subsequently enhanced, with K playing a major role at 200 hPa but K_R always determining the vertical distribution of K. The contribution of K_D and K_{RD} to K is small, and K_{RD} makes a negative contribution to K. The distribution and variation of K and K_R are greatest at 200 hPa; therefore, we focused on K and K_R at 200 hPa.

Figure 4 shows the horizontal distribution of K and K_R at 200 hPa. As can be seen from Figs. 4a–c, the horizontal distribution of K is very similar to that of K_R. Both are continuously enhanced, indicating the upper-level shortwave trough in the west of the torrential-rain area and the upper-level jet in the east were strengthened (figure omitted). This promoted the vertical motion of the torrential-rain area (figure omitted), and the ETR was subsequently enhanced. During the initial stage (Fig. 4a), both K and K_R are 40 J m^{-2}, which both then increase to 120 J m^{-2} during the rapid increase stage (Fig. 4b), and to 200 J m^{-2} and 240 J m^{-2}, respectively, during the maintenance stage (Fig. 4c).

In summary, during this ETR process, K was enhanced, and subsequently so too was the ETR. Also, the distribution and variation of K were greatest at 200 hPa, where K was mainly derived from K_R. The enhancement of K and K_R at 200 hPa in the torrential-rain area enhanced the vertical motion and then favored the enhancement of ETR.

3.3. *Relationship between K and hourly precipitation intensity*

As can be seen in Fig. 5, the magnitude and evolutionary

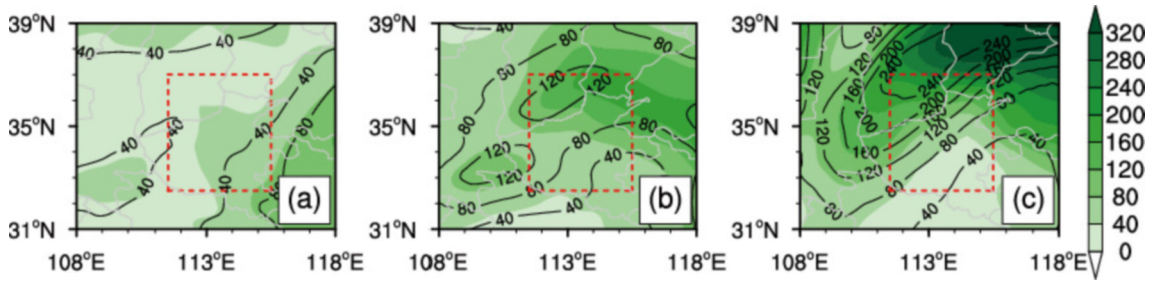

Fig. 4. Horizontal distributions of K (shaded) and K_R (contours) at 200 hPa (units: J m^{-2}) in the (a) initial stage, (b) rapid increase stage, and (c) maintenance stage.

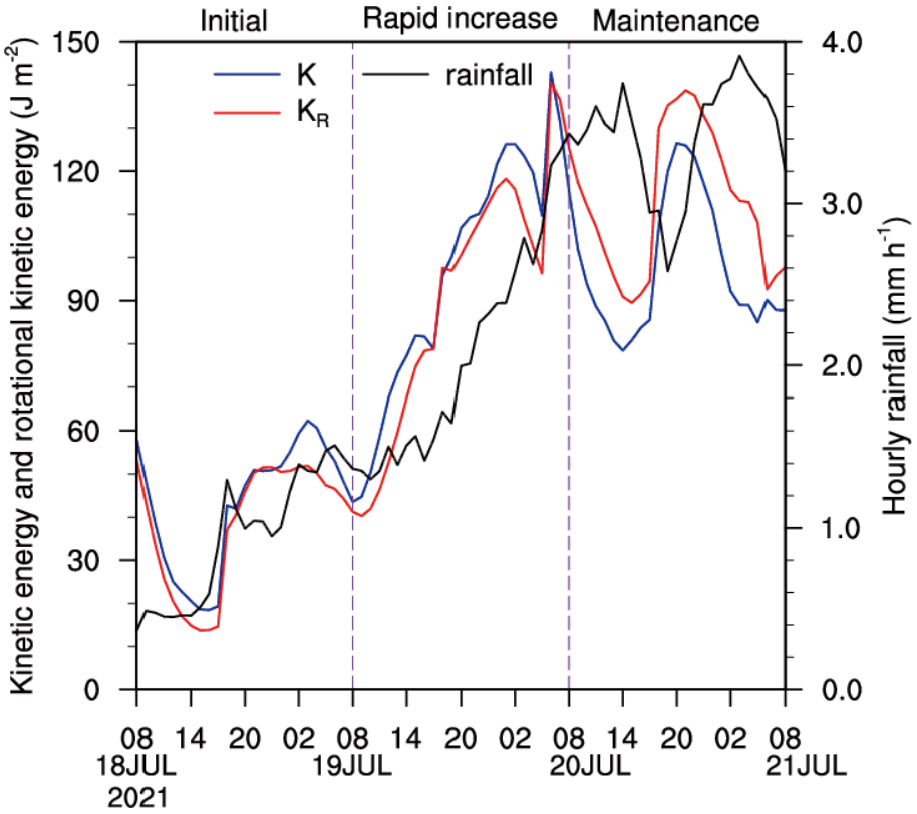

Fig. 5. Temporal evolution of the area-averaged hourly precipitation (black line; units: mm h^{-1}), K (blue line, units: J m^{-2}), and K_R (red line, units: J m^{-2}) at 200 hPa in the torrential-rain area.

trend of K at 200 hPa are close to those of K_R, and the enhancement of both promotes the enhancement of ETR. Using Pearson correlation coefficients, we calculated the simultaneous temporal correlation coefficients of K and K_R for the regional average of the torrential-rain area at 200 hPa with the hourly precipitation intensity, respectively, which revealed the correlation coefficient of K_R with the hourly precipitation intensity to be much larger, at up to 0.9, which was statistically significant at the 0.01 confidence level, based on a Student's t-test. This shows that K_R has a stronger correlation with the hourly precipitation intensity. During the initial stage, both K_R and the hourly precipitation intensity slowly; during the rapid increase stage, they both intensify sharply; and during the maintenance stage, they both show fluctuating changes and maintain high values. The evolution of K_R is ahead of the hourly precipitation intensity in the ETR process, and this advance is largest (~8 h) in the maintenance stage, which indicates that K_R could perhaps serve as a predictor of ETR development.

In conclusion, K_R was most closely related to the hourly precipitation intensity at 200 hPa, with a correlation coefficient as high as 0.9. The K_R at 200 hPa could perhaps be used to predict the hourly precipitation intensity 8 h in advance at the earliest, and thus could serve as a predictor of the ETR. Therefore, the rotational kinetic energy equation was used to diagnose the ETR process.

3.4. *Rotational kinetic energy budget*

According to Fig. 6a and Table 1, during the initial stage, DK_R presents a distribution of "positive in the west

and negative in the east", with a regional average value of 0.4×10^{-4} W m^{-2} Pa^{-1}. During the rapid increase stage, the positive-value area of DK_R expands and covers the whole torrential-rain area, with a regional average value of 11.46×10^{-4} W m^{-2} Pa^{-1} (Fig. 6b and Table 1). During the maintenance stage, the absolute values of DK_R are relatively small over the whole torrential-rain area, with a regional average value of -1.9×10^{-4} W m^{-2} Pa^{-1} (Fig. 6c and Table 1). This shows that K_R increased slowly in the initial stage, rapidly increased in the rapid increase stage, and maintained a high value in the maintenance stage.

Diagnosis shows that the regional average values of the conversion term G_R between available energy and K_R, F_R, and I_R are always positive, which is beneficial to the enhancement of K_R, and the regional average values of HF_R, C (K_D, K_R), are always negative, which is beneficial to the reduction of K_R (Table 1). During the initial stage, the positive-value area of F_R covers the torrential-rain area (Fig. 6j), and its regional average value of 3.47×10^{-4} W m^{-2} is conducive to the enhancement of K_R. Meanwhile, G_R (Fig. 6a) and I_R

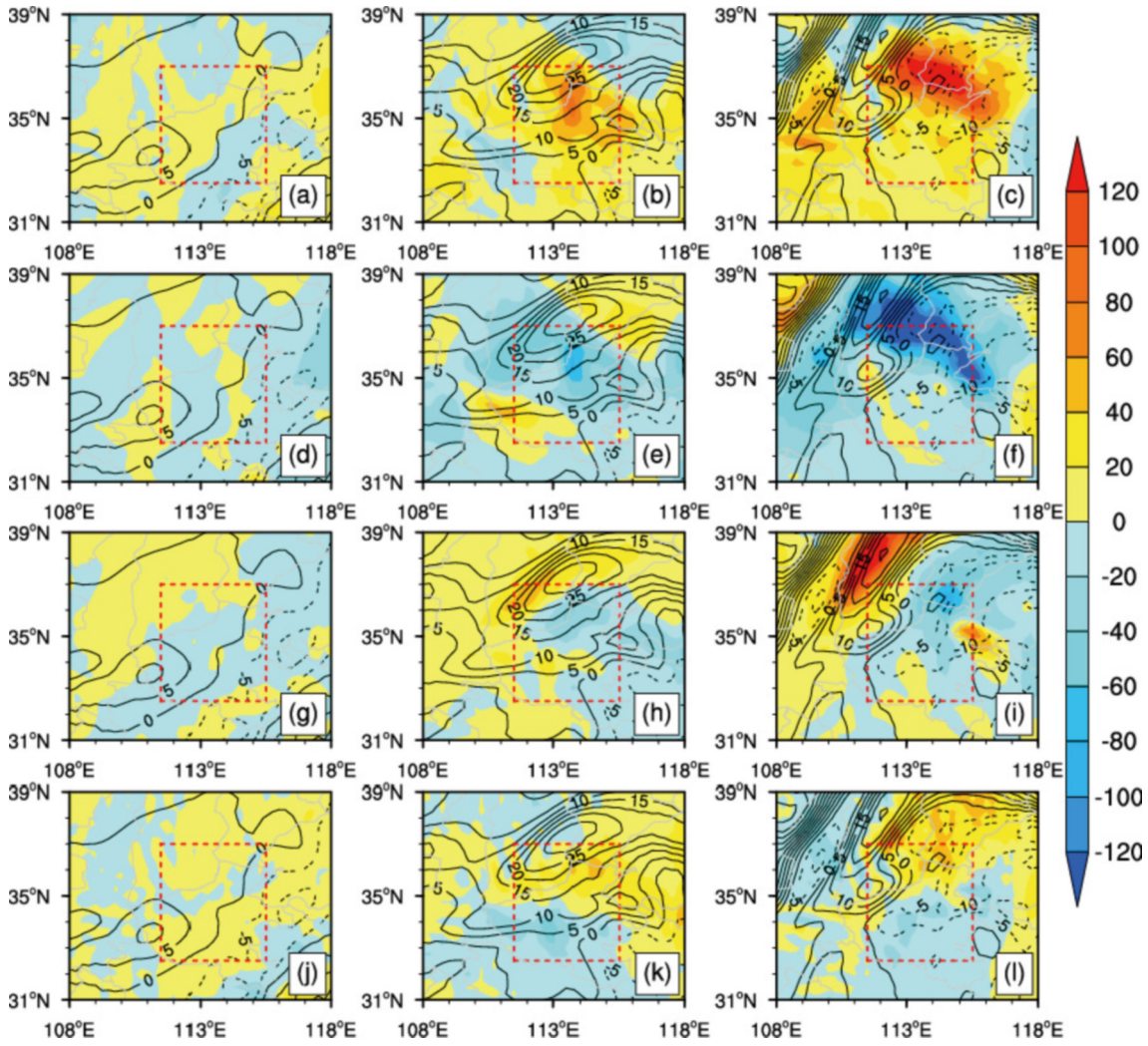

Fig. 6. Horizontal distribution of the local variation in K_R (DK_R) (contours; units: 10^{-4} W m^{-2} Pa^{-1}): (a–c) the conversion between APE and K_R (G_R); (d–f) the horizontal flux divergence of K by V_R (HF_R); (g–i) the conversion between K_R and K_D [$C(K_D, K_R)$]; and (j–l) the friction term related to V_R (F_R) (shaded; units: 10^{-4} W m^{-2} Pa^{-1}) at 200 hPa. Panels (a, d, g, j) present the initial stage, (b, e, h, k) present the rapid increase stage, and (c, f, i, l) present the maintenance stage.

Table 1. Reginal average budget of K_R in the torrential-rain area at 200 hPa (units: 10^{-4} W m^{-2} Pa^{-1}).

Period	DK_R	G_R	HF_R	F_R	C (K_D, K_R)	I_R
Initial stage	0.40	0.21	−3.02	3.47	−0.98	0.71
Rapid increase stage	11.46	26.50	−20.66	2.88	−2.59	5.33
Maintenance stage	−1.9	44.6	−40.44	1.76	−9.04	1.23

(figure omitted) have less beneficial effects, indicating kinetic energy transfer from the sub-grid to grid scale, leading to the slow increase in K_R in the initial stage. During the rapid increase stage, the positive-value range of G_R expands and concentrates in the north-central part of the torrential-rain area (Fig. 6b), and its regional average value increases to 26.5×10^{-4} W m^{-2} Pa^{-1}, which is conducive to the enhancement of K_R. Meanwhile, the beneficial effects of F_R (Fig. 6k) and I_R (figure omitted) are far less than those of G_R, indicating that the pressure gradient force does positive work, so that the APE can be converted into K_R through the barotropic process, leading to the enhancement of K_R. During the maintenance stage, the absolute values of G_R, HF_R, and $C(K_D, K_R)$ increase significantly (Figs. 6f, i and l). As can be seen from Table 1, the regional average value of G_R increases to 44.6×10^{-4} W m^{-2} Pa^{-1}, which can generate K_R, indicating that the conversion of the APE to K_R through the barotropic process is enhanced. However, the regional average value of HF_R decreases to -40.44×10^{-4} W m^{-2} Pa^{-1}, indicating that the horizontal transportation of K by $\boldsymbol{V}_R$ is a net output, which will consume K_R (Table 1). Therefore, under the joint action of G_R and HF_R, the high value of K_R is maintained.

In conclusion, during the initial stage, F_R dominated the slow enhancement of K_R. During the rapid increase stage, G_R dominated the rapid enhancement of K_R, which was conducive to the rapid enhancement of ETR. During the maintenance stage, G_R and HF_R jointly maintained a high value of K_R, which was conducive to the maintenance of ETR.

It can be seen from the above that ETR was mainly concentrated in the rapid increase stage and the maintenance stage. Therefore, we further discuss the physical meaning of the main contributing terms during the rapid increase stage and the maintenance stage. In the rapid increase stage, the geopotential height is distributed with a "lower in the north and higher in the south" pattern, and the rotational wind is an anticyclonic southwesterly wind. When the meridional rotational wind (u_R) crosses the isobar from south to north, the pressure gradient force does positive work. Therefore, the joint action of u_R and the meridional geopotential gradient controls the conversion of APE to K_R through the barotropic process, leading to the rapid enhancement of K_R during this stage (Fig. 7a). During the maintenance stage, the meridional potential gradient and the rotational wind continue to increase, which leads to the enhancement of the conversion of APE to K_R through the barotropic process (Fig. 7b). At the same time, the value of K in the southwest of the torrential-rain area is relatively small, while the value in the northeast of the torrential-rain area is relatively large (Fig. 7c). Therefore, the anticyclonic rotational wind transports K from the southwest to the northeast of the torrential-rain area, consuming K_R.

In conclusion, during the ETR process, the conversion of kinetic energy from the sub-grid to grid scale made the ETR develop slowly. The APE was converted into K_R through a barotropic process, leading to a sharp enhancement of K_R, which was conducive to the sharp enhancement of ETR. K_R was consumed owing to the outward transportation of K in the rotational wind direction, which basically offset the K_R produced by the barotropic process. Therefore, the high value of K_R was basically maintained, which was conducive to the maintenance of ETR. Furthermore, the conversion of APE to K_R through the barotropic process depended on the joint action of the meridional rotational wind and the meridional potential gradient.

4. Discussion and conclusions

Based on ERA5 reanalysis data and hourly precipitation data from meteorological stations in China, the ETR event that occurred in Henan Province, China, 18–21 July 2021, was investigated from the perspective of kinetic energy. According to the regional hourly precipitation intensity variability in the torrential-rain area, the ETR process was divided into an initial stage, a rapid increase stage, and a maintenance stage. The spatial and temporal distribution of K and its relationship with hourly rainfall intensity was discussed, and the mechanism of ETR enhancement and maintenance was diagnosed using the rotational wind kinetic energy equation. The study addresses the lack of mechanistic research on the 21·7 ETR from a kinetic energetic view-

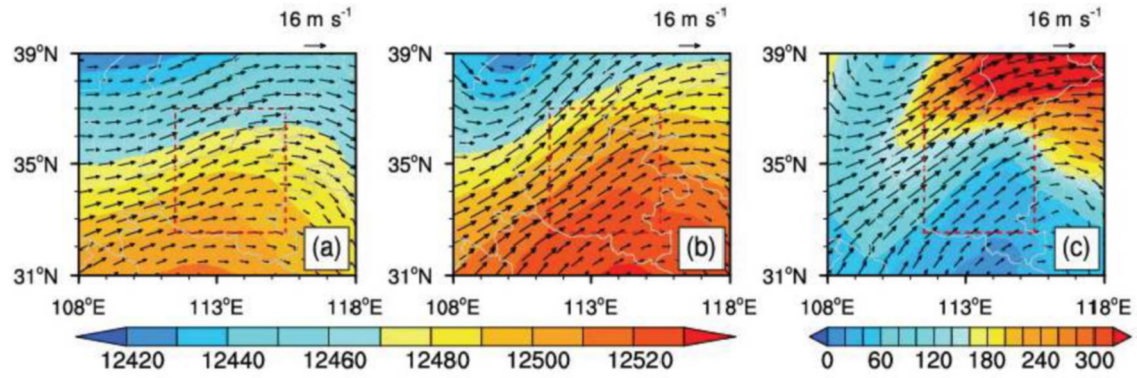

Fig. 7. Horizontal distribution of the (a–c) rotational wind (vector arrows; units: m s^{-1}), (a, b) geopotential height (shaded; units: gpm), and (c) K (shaded; units: J m^{-2}) at 200 hPa in the (a) rapid increase stage and (b, c) maintenance stage.

point, and provides a reference for the forecasting and early warning of torrential rainstorms. The main conclusions are:

(1) During the 21·7 ETR process, K and its variation were largest at 200 hPa, and K mainly derived from K_R.

(2) The evolution of K_R at 200 hPa was most closely related to the hourly rainfall intensity during the ETR process, and the correlation coefficient was as high as 0.9. In particular, the peak value of K_R was 8 h ahead of the hourly rainfall intensity, which has a certain significance for indicating the development and maintenance of ETR.

(3) The conversion of kinetic energy from the sub-grid to grid scale made the ETR develop slowly during the initial stage. The APE was converted into K_R through the barotropic process, leading to a sharp enhancement of K_R, which was conducive to the sharp enhancement of ETR during the rapid increase stage. Furthermore, the conversion of APE to K_R depended on the joint action of the meridional rotational wind and the meridional potential gradient. During the maintenance stage, K_R was consumed owing to the outward transportation of K in the rotational wind direction, which basically offset the K_R produced by the barotropic process. Therefore, the high value of K_R was basically maintained, which was conducive to the maintenance of ETR.

From the perspective of K, our research diagnoses the 21·7 ETR process and further improves the level of understanding regarding the enhancement and maintenance mechanism of this event. The intensification of the horizontal gradient of geopotential height caused by a cold low may result in the increase of K_R in the upper troposphere, which indicates enhanced upper-level anticyclonic circulation in the torrential-rain area (Cai et al., 2022).

However, many scientific issues worth exploring remain. For example, the divergent flow was formed to the right of the jet entrance, which strengthened the local ascending motion and induced a lower-level vortex, causing the rain peak during the ETR (Fu et al., 2022). The interaction of the lower-level, middle-level, and upper-level K_R and K_D. may be the reason why the peak of K_R was found to be 8 h ahead of the rainfall intensity during the ETR. Therefore, the balance of K and the conversion between K_D and K_R at different levels during the ETR process are deserving of further study.

Acknowledgements. This study was jointly supported by the National Natural Science Foundation of China (Grant Nos. 42275013, 42030611 and 42175008) and the Open Grants of the State Key Laboratory of Severe Weather (Grant No. 2021LASW-B17).

REFERENCES

Bao, X. H., and X. P. Yao, 2022: Intensity evolution of zonal shear line over the Tibetan Plateau in summer: A perspective of divergent and rotational kinetic energies. *Adv. Atmos. Sci.*, **39**(7), 1021−1033, https://doi.org/10.1007/s00376-021-1302-9.

Buechler, D. E., and H. E. Fuelberg, 1986: Budgets of divergent and rotational kinetic energy during two periods of intense convection. *Mon. Wea. Rev.*, **114**(1), 95−114, https://doi.org/10.1175/1520-0493(1986)114<0095:BODARK>2.0.CO;2.

Bueh, C., A. R. Zhuge, Z. W. Xie, Z. T. Gao, and D. W. Lin, 2022: Water vapor transportation features and key synoptic-scale systems of the "7.20" rainstorm in Henan Province in 2021. *Chinese Journal of Atmospheric Sciences*, **46**(3), 725−744, https://doi.org/10.3878/j.issn.1006-9895.2202.21226. (in Chinese with English abstract)

Cai, X. N., T. Chen, Y. Zhan, J. L. Fu, and N. Hu, 2022: Dynamic impact of upper tropospheric cold low on persistent extreme rainstorm of Henan during 17−22 July 2021. *Meteorological Monthly*, **48**(5), 545−555, https://doi.org/10.7519/j.issn.1000-0526.2022.021802. (in Chinese with English abstract)

Chen, G., and Coauthors, 2022: Variability of microphysical characteristics in the "21·7 " Henan extremely heavy rainfall event. *Science China Earth Sciences*, **65**(10), 1861−1878, https://doi.org/10.1007/s11430-022-9972-9.

Cheng, Z. Q., L. X. Lin, Y. Liu, and G. J. Yang, 2014: Analysis on the wind kinetic of divergence energy of torrential rain in East Guangdong associated with Typhoon Noguri. *Plateau Meteorology*, **33**(2), 557−566, https://doi.org/10.7522/j.issn.1000-0534.2013.00019. (in Chinese with English abstract)

Chyi, D., L. F. He, X. M. Wang, and S. Chen, 2022: Fine observation characteristics and thermodynamic mechanisms of extreme heavy rainfall in Henan on 20 July 2021. *Journal of Applied Meteorological Science*, **33**(1), 1−15, https://doi.org/10.11898/1001-7313.20220101. (in Chinese with English abstract)

Cui, X. P., and Y. T. Yang, 2022: Tracking and quantitative contribution analyses of moisture sources of rainstorm in Henan Province in July 2021. *Chinese Journal of Atmospheric Sciences*, **46**(6), 1543−1556, https://doi.org/10.3878/j.issn.1006-9895.2203.22016. (in Chinese with English abstract)

Deng, D. F., Y. S. Zhou, and D. H. Wang, 2012: The application of wind and water-vapor flux partitioning technique to the structure of a northeast vortex in 2006. *Chinese Journal of Geophysics*, **55**(6), 1852−1866, https://doi.org/10.6038/j.issn.0001-5733.2012.06.006. (in Chinese with English abstract)

Deng, L., J. N. Feng, Y. Zhao, X. W. Bao, W. Huang, H. Hu, and Y. H. Duan, 2022: The remote effect of binary Typhoon Infa and Cempaka on the "21.7 " heavy rainfall in Henan Province, China. *J. Geophys. Res. Atmos.*, **127**(16), e2021JD036260, https://doi.org/10.1029/2021JD036260.

Ding, Y. H., and Y. Z. Liu, 1985: On the analysis of typhoon kinetic energy-Conversion between divergent and nondivergent wind. *Science in China* (*Series B*), **15**(11), 1045−1054, https://doi.org/10.1360/zb1985-15-11-1045. (in Chinese with English abstract)

Disaster Investigation Group of the State Council, 2022: A report on an investigation into the disaster caused by "7·20" torrential rains in Zhengzhou, Henan Province. 44 pp. (in Chinese)

Duan, T., Q. L. Chen, and Y. J. Liao, 2022: Analysis of "21.7" extreme rainstorm formation process and disaster mechanism in Zhengzhou. *Journal of the Meteorological Sciences*, **42**(2), 152−161. (in Chinese with English abstract)

Duan, X., Sun, J. H., and Z. X. Wang, 1997: Comparing characteristics of budget for divergent and rotational components of kinetic energy in heavy rain and no-heavy rain processes. *Plateau Meteorology*, **1**(2), 93−98, https://doi.org/10.1088/0256-307X/13/9/012. (in Chinese with English abstract)

Endlich, R. M., 1967: An iterative method for altering the kinematic properties of wind fields. *J. Appl. Meteorol.*, **6**, 837–844, https://doi.org/10.1175/1520-0450(1967)006<0837:AIMFAT>2.0.CO;2.

Fu, S. M., J. H. Sun, S. X. Zhao, and W. L. Li, 2011: The energy budget of a southwest vortex with heavy rainfall over south China. *Adv. Atmos. Sci.*, **28**(3), 709–724, https://doi.org/10.1007/s00376-010-0026-z.

Fu, S. M., J. H. Sun, J. Ling, H. J. Wang, and Y.C. Zhang, 2016: Scale interactions in sustaining persistent torrential rainfall events during the Mei-yu season. *J. Geophys. Res. Atmos.*, **121**(21), 12 856–12 876, https://doi.org/10.1002/2016JD025446.

Fu, S.-M., Y.-C. Zhang, H.-J. Wang, H. Tang, W.-L. Li, and J.-H. Sun, 2022: On the evolution of a long-lived mesoscale convective vortex that acted as a crucial condition for the extremely strong hourly precipitation in Zhengzhou. *J. Geophys. Res. Atmos.*, **127**(11), e2021JD036233, https://doi.org/10.1029/2021JD036233.

Fuelberg, H. E., and P. A. Browning, 1983: Roles of divergent and rotational winds in the kinetic energy balance intense convective activity. *Mon. Wea. Rev.*, **111**(11), 2176–2193, https://doi.org/10.1175/1520-0493(1983)111<2176:RODARW>2.0.CO;2.

Hersbach, H., and Coauthors, 2020: The ERA5 global reanalysis. *Quart. J. Roy. Meteor. Soc.*, **146**(730), 1999–2049, https://doi.org/10.1002/qj.3803.

Jin, S. L., S. L. Feng, W. Shen, S. M. Fu, L. Z. Jiang, and J. H. Sun, 2020: Energetics characteristics accounting for the low-level wind's rapid enhancement associated with an extreme explosive extratropical cyclone over the western North Pacific Ocean. *Atmos. Ocean. Sci. Lett.*, **13**(5), 426–435, https://doi.org/10.1080/16742834.2020.1763153.

Li, S. S., and S. W. Shou, 1995: Energetic of maintenance and rainfall amplification of landed Typhoons. *Journal of Nanjing Institute of Meteorology*, **18**(3), 383–388. (in Chinese with English abstract)

Liang, X. D., and Coauthors, 2022: Preliminary investigation on the extreme rainfall event during July 2021 in Henan Province and its multi-scale processes. *Chinese Science Bulletin*, **67**(11), 997–1011, https://doi.org/10.1360/TB-2021-0827. (in Chinese with English abstract)

Luo, Y. H., and Y. Du, 2023: The roles of low-level jets in "21·7" Henan extremely persistent heavy rainfall event. *Adv. Atmos. Sci.*, **40**(3), 350–373, https://doi.org/10.1007/s00376-022-2026-1.

Nie, Y. B., and J. Q. Sun, 2022: Moisture sources and transport for extreme precipitation over Henan in July 2021. *Geophys. Res. Lett.*, **49**(4), e2021GL097446, https://doi.org/10.1029/2021GL097446.

Pearce, R. P., 1974: The design and interpretation of diagnostic studies of synoptic scale atmospheric system. *Quart. J. Roy. Meteor. Soc.*, **100**(425), 265–285, https://doi.org/10.1002/qj.49710042502.

Qin, H., W. Yuan, J. Wang, Y. Chen, P. X. Dai, A. H. Sobel, Z. Y. Meng, and J. Nie. 2022: Climate change attribution of the 2021 Henan extreme precipitation: Impacts of convective organization. *Science China Earth Sciences*, **65**(10), 1837–1846, https://doi.org/10.1007/s11430-022-9953-0.

Ran, L. K., and Coauthors, 2021: Observational analysis of the dynamic, thermal, and water vapor characteristics of the "7.20" extreme rainstorm event in Henan Province, 2021. *Chinese Journal of Atmospheric Sciences*, **45**(6), 1366–1383, https://doi.org/10.3878/j.issn.1006-9895.2109.21160. (in Chinese with English abstract)

Sha, S., X. Y. Shen, and X. F. Li, 2018: The study of multi-scale energy interactions during a Meiyu front rainstorm. Part II: Practical application. *Chinese Journal of Atmospheric Sciences*, **42**(5), 1119–1132, https://doi.org/10.3878/j.issn.1006-9895.1710.17196. (in Chinese with English abstract)

Su, A. F, X. N. Lü, L. M. Cui, Z. Li, L. Xi, and H. Li, 2021: The basic observational analysis of "7.20" extreme rainstorm in Zhengzhou. *Torrential Rain and Disasters*, **40**(5), 445–454, https://doi.org/10.3969/j.issn.1004-9045.2021.05.001. (in Chinese with English abstract)

Sun, S. Q., S. C. Tian., and C. X. Du, 1993: The features of flow pattern in upper level troposphere and energy conversion during the development of meso-scale low vortex. *Chinese Journal of Atmospheric Sciences*, **17**(2), 137–147, https://doi.org/10.3878/j.issn.1006-9895.1993.02.02. (in Chinese with English abstract)

Sun, Y., H. Xiao, H. L. Yang, J. F. Ding, D. H. Fu, X. L. Guo, and L. Feng, 2021: Analysis of dynamic conditions and hydrometeor transport of Zhengzhou superheavy rainfall event on 20 July 2021 based on optical flow field of remote sensing data. *Chinese Journal of Atmospheric Sciences*, **45**(6), 1384–1399, https://doi.org/10.3878/j.issn.1006-9895.2109.21155. (in Chinese with English abstract)

Wang, J., D. Wu, C. J. Wang, L. Xi, and L. Liu, 2022: Analysis on the influence of distance typhoon on the extreme precipitation in July 2021 in Henan. *Meteorological and Environmental Sciences*, **45**(2), 75–85, https://doi.org/10.16765/j.cnki.1673-7148.2022.02.008. (in Chinese with English abstract)

Wang, Y. P., X. P. Cui, X. F. Li, W. L. Zhang, and Y. J. Huang, 2016: Kinetic energy budget during the genesis period of tropical cyclone durian (2001) in the South China Sea. *Mon. Wea. Rev.*, **144**(8), 2831–2854, https://doi.org/10.1175/MWR-D-15-0042.1.

Wang, Z. X., 1993: The characteristics of conversion between kinetic energies of divergent winds and non-divergent winds during heavy rain period. *Chinese Journal of Atmospheric Sciences*, **17**(2), 185–191, https://doi.org/10.3878/j.issn.1006-9895.1993.02.07. (in Chinese with English abstract)

Wang, Z. X., and Y. Liu, 1994: The budgets of rotational and divergent component of kinetic energy for subsynoptic scale vortex at the Mei-Yu front. *Plateau Meteor.*, **13**(1), 28–34, https://doi.org/10.1007/BF02658170. (in Chinese with English abstract)

Xie, A., W. J. Xiao, and S. J. Chen, 1980: Kinetic energy budget of sub-synoptic scale disturbance during Mei-Yu season. *Acta Meteorologica Sinica*, **38**(4), 351–359, https://doi.org/10.11676/qxxb1980.041. (in Chinese with English abstract)

Xu, H. X., Y. H. Duan, and X. D. Xu, 2022a: Indirect effects of binary typhoons on an extreme rainfall event in Henan province, China from 19 to 21 July 2021: 1. Ensemble-based analysis. *J. Geophys. Res. Atmos.*, **127**(10), e2021JD036265, https://doi.org/10.1029/2021JD036265.

Xu, J., R. M. Li, Q. H. Zhang, Y. Chen, X. D. Liang, and X. J. Gu, 2022b: Extreme large-scale atmospheric circulation associated with the "21·7" Henan flood. *Science China Earth Sciences*, **65**(10), 1847–1860, https://doi.org/10.1007/s11430-022-9975-0.

Yin, J. F., H. D. Gu, X. D. Liang, M. Yu, J. S. Sun, Y. X. Xie, F. Li, and C. Wu, 2022: A possible dynamic mechanism for

rapid production of the extreme hourly rainfall in Zhengzhou City on 20 July 2021. *J. Meteor. Res.*, **36**(1), 6–25, https://doi.org/10.1007/s13351-022-1166-7.

Yu, Y. B., and X. P. Yao, 1999: Diagnosis of "96.8" torrential rain with the scale-seperation kinetic energy equation. *Journal of Applied Meteorological Science*, **10**(1), 49–58, https://doi.org/10.3969/j.issn.1001-7313.1999.01.007. (in Chinese with English abstract)

Zhang, G. S., J. Y. Mao, W. Hua, X. F. Wu, R. Z. Sun, Z. Y. Yan, Y. M. Liu, and G. X. Wu, 2023: Synergistic effect of the planetary-scale disturbance, typhoon and meso-β-scale convective vortex on the extremely intense rainstorm on 20 July 2021 in Zhengzhou. *Adv. Atmos. Sci.*, **40**, 428–446, https://doi.org/10.1007/s00376-022-2189-9.

Zhang, S. H., Y. R. X. Chen, Y. L. Luo, B. Liu, G. Y. Ren, T. J. Zhou, C. Martinez-Villalobos, and M. Y. Chang, 2022: Revealing the circulation pattern most conducive to precipitation extremes in Henan Province of North China. *Geophys. Res. Lett.*, **49**(7), e2022GL098034, https://doi.org/10.1029/2022GL098034.

Zhang, X., H. Yang, X. M. Wang, L. Shen, D. Wang, and H. Li, 2021: Analysis on characteristic and abnormality of atmospheric circulations of the July 2021 extreme precipitation in Henan. *Transactions of Atmospheric Sciences*, **44**(5), 672–687, https://doi.org/10.13878/j.cnki.dqkxxb.20210907001. (in Chinese with English abstract)

Zhao, Y., L. Deng, Z. W. Li, and Y. J. Wang, 2022: Quantitative attribution of vertical motion responsible for summer heavy rainfall over North China. *J. Geophys. Res. Atmos.*, **127**(2), e2021JD035765, https://doi.org/10.1029/2021JD035765.

Zhong, S.-X., W.-G. Meng, and F.-Y. Tian, 2021: Budgets of rotational and divergent kinetic energy in the warm-sector torrential rains over South China: A case study. *Meteorol. Atmos. Phys.*, **133**(3), 759–769, https://doi.org/10.1007/s00703-021-00778-1.

Zhu, C. D., Z. H. Chen, Y. F. Li, Y. Xu, G. S. Zhang, and J. Liao, 2022: Effects of stratospheric high PV intrusion on the July 2021 extremely severe torrential rain in Henan Province. *Meteorological and Environmental Sciences*, **45**(2), 27–37, https://doi.org/10.16765/j.cnki.1673-7148.2022.02.004. (in Chinese with English abstract)